Radiol Phys Technol (2017) 10:422–430
https://doi.org/10.1007/s12194-017-0414-5

Effects of a novel tungsten-impregnated rubber neck shield on the quality of cerebral images acquired using ^{15}O-labeled gas

Kei Wagatsuma[1,2] · Keiichi Oda[1,3] · Kenta Miwa[4] · Motoki Inaji[1,5] · Muneyuki Sakata[1] · Jun Toyohara[1] · Kiichi Ishiwata[1,6,7] · Masayuki Sasaki[2] · Kenji Ishii[1]

Received: 17 May 2017 / Revised: 11 August 2017 / Accepted: 14 August 2017 / Published online: 19 August 2017

Abstract The present study aimed to validate the effects of a novel tungsten-impregnated rubber neck shield on the quality of phantom and clinical ^{15}O-labeled gas positron emission tomography (PET) images. Images were acquired in the presence or absence of a neck shield from a cylindrical phantom containing [^{15}O]H_2O (phantom study) and from three individuals using [^{15}O]CO_2, [^{15}O]O_2 and [^{15}O]CO gas (clinical study). Data were acquired in three-dimensional (3D) mode using a Discovery PET/CT 710. Values for cerebral blood flow, cerebral blood volume, oxygen extraction fraction, and cerebral metabolic rate of oxygen with and without the neck shield were calculated from ^{15}O-labeled gas images. Arterial radioactivity and count characteristics were evaluated in the phantom and clinical studies. The coefficient of variance (CV) for the phantom study and the standard deviation (SD) for functional images were also analyzed. The neck shield decreased the random count rates by 25–59% in the phantom and clinical studies. The noise equivalent count rate (NECR) increased by 44–66% in the phantom and clinical studies. Random count rates and NECR in [^{15}O]CO_2 images significantly differed with and without the neck shield. The improvement in visual and physical image quality with the neck shield was not observed in the phantom and clinical studies. The novel neck shield reduced random count rate and improved NECR in a 3D PET study using ^{15}O-labeled gas. The image quality with the neck shield was similar to that without the neck shield.

Keywords Positron emission tomography · Oxygen-15 · Image quality · Count characteristics · Neck shield

✉ Kenji Ishii
Ishii@pet.tmig.or.jp

1 Research Team for Neuroimaging, Tokyo Metropolitan Institute of Gerontology, 35-1, Sakae-cho, Itabashi-ku, Tokyo 173-0015, Japan

2 Department of Health Sciences, Graduate School of Medical Science, Kyushu University, Fukuoka, Japan

3 Faculty of Health Science, Hokkaido University of Science, Sapporo, Japan

4 School of Health Science, International University of Health and Welfare, Ohtawara, Japan

5 Department of Neurosurgery, Tokyo Medical and Dental University, Tokyo, Japan

6 Institute of Cyclotron and Drug Discovery Research, Southern TOHOKU Research Institute for Neuroscience, Koriyama, Japan

7 Department of Biofunctional Imaging, Fukushima Medical University, Fukushima, Japan

1 Introduction

Cerebral blood flow (CBF), cerebral blood volume (CBV), oxygen extraction fraction (OEF), and cerebral metabolic rate of oxygen ($CMRO_2$) have been quantified by positron emission tomography (PET) using oxygen-15-labeled gases [1–3]. These quantitative parameters have been applied to pathophysiological evaluations and used to predict outcomes among patients with cerebral vascular disease [4–7].

Newer PET scanners comprised of lutetium-based scintillator acquire data only in three-dimensional (3D) mode, which is optimized for whole-body scanning. The high sensitivity of 3D PET has decreased the acquisition time and the radiation dose associated with whole-body imaging [8, 9]. However, the increase in scattered photons from radioactivity outside the field of view (FOV) not only

degrades image quality but also decreases the quantitative accuracy of 3D PET [10–16]. Direct and scatter photons from large amounts of ^{15}O in the lungs and in blood pools, such as the heart and major blood vessels, affect quantitative PET measurements. Neck shields have been developed to reduce the contribution of annihilation photons from outside the FOV [11, 15, 17–19]. Ibaraki et al. found that an additional neck shield made of lead plate reduced random events and improved the signal-to-noise ratio (SNR) derived from reconstructed image-based SNRs generated by 3D PET using ^{15}O-labeled compounds [15]. Lutetium-based scintillators such as lutetium–yttrium–orthosilicate (LYSO) and Lu_2SiO_5 (LSO) have faster scintillation decay than $Bi_4Ge_3O_{12}$ (BGO) and Gd_2SiO_5 (GSO) [20]. The high count-rate capability of LYSO scintillator reduces dead time and random coincidence events. However, Kloet et al. proposed that an additional neck shield would reduce the effects of radioactivity outside the FOV even when images are acquired using a PET scanner with LSO [16].

Previous neck shields have been made of lead plate [11, 15–17, 19]. We previously used the lead-plate neck shield used by Ibaraki et al. [15] during a ^{15}O-labeled gas study using a conventional PET scanner that has a smaller trans-axial FOV than do most PET/CT scanners. The neck shield made of lead could be attached to PET scanners manufactured by SHIMADZU (SHIMADZU Corp., Kyoto, Japan) only [15]. In the present study, we used a novel neck shield comprised of tungsten-impregnated rubber and a stainless metal-alloy frame to reduce scatter radiation from radioactivity outside the FOV. Tungsten-impregnated rubber is softer and more flexible than lead; it can be shaped to fit curved surfaces. The neck shield was designed to avoid feelings of oppression and constriction during ^{15}O-labeled gas studies regardless of the physique of the patient.

The present study aimed to validate the effects of the tungsten-impregnated rubber neck shield on the quality of images acquired from a phantom (phantom study) and from ^{15}O-labeled gas inhalation (clinical study) using 3D PET and a high-end LYSO scanner.

2 Materials and methods

2.1 PET/CT equipment

All data were acquired using a Discovery PET/CT 710 (GE Healthcare, Milwaukee, WI, USA) [21]. The PET scanner comprised 13,824 LYSO crystals in a 4.2 × 6.3 × 25-mm^3 block. The PET detector comprised a 150.42-mm axial FOV and a 700-mm trans-axial FOV with a 64-slice CT scanner. The spatial resolution according to the National Electrical Manufacturers Association (NEMA) NU 2-2007 was 4.52 mm (full width at half maximum, FWHM, at 1.0 cm off center) [22].

2.2 Novel neck shield

The novel neck shield (Universal Giken, Odawara, Japan) comprised a stainless alloy frame with an axial length of 163 mm and tungsten-impregnated rubber (6 mm thick) that was equivalent to >6 mm lead (Fig. 1). The 564 × 318 mm (width and height) rubber component consists of a base sheet, right and left covers, and top sheet that are easily connected and can cover the shoulders of patients. The weights of the neck shield components were 6.6, 5.6, and 3.6 kg for the base sheet, right and left covers, and top sheet, respectively.

2.3 Phantom study

An acrylic cylindrical phantom (diameter, 20 cm; length, 16 cm) simulated a human head and another (diameter, 20 cm; length, 25 cm) simulated the body. The center of the PET axial FOV head-simulated phantom containing $[^{15}O]H_2O$ was placed 16 cm from the body phantom containing an ^{18}F solution. The reported brain to body radioactivity ratio of inhaled $[^{15}O]O_2$ is 1:8 [23]. The radioactivity ratio of brain to body was set to 1:7.6 and 1:7.3 with and without neck shield, respectively, at the start of each image acquisition. The amount of $[^{15}O]H_2O$ radioactivity in the head-simulated phantom was determined by the mean radioactive concentration of the whole brain in the $[^{15}O]O_2$ images of three participants. The amount of radioactivity was 102.9 and 93.7 MBq with and without the neck shield, respectively, at the start of each image acquisition. Images were acquired from the head-simulated phantom for 3.5 min with and without the neck shield.

2.4 Clinical study

All retrospective experiments were approved by the institutional review board (IRB) and were performed in accordance with the IRB rules and policies (282559, and 28-371). We retrospectively analyzed ^{15}O-labeled gas images acquired from three participants (average age, 22.5 years; average height, 172.0 cm; average weight, 64.0 kg). After a low-dose CT scan for attenuation correction, three sequential emission scans of inhaled $[^{15}O]CO_2$ (2000 MBq/min), $[^{15}O]O_2$ (3000 MBq/min), and $[^{15}O]CO$ (2000 MBq/min) were performed with and without the neck shield (Fig. 2). The acquisition of images for 3.5 min in $[^{15}O]CO_2$ and $[^{15}O]O_2$ scans were initiated simultaneously with the 1.5-min inhalation of these gases [24]. Then, participants inhaled $[^{15}O]CO$ gas for 4 min and

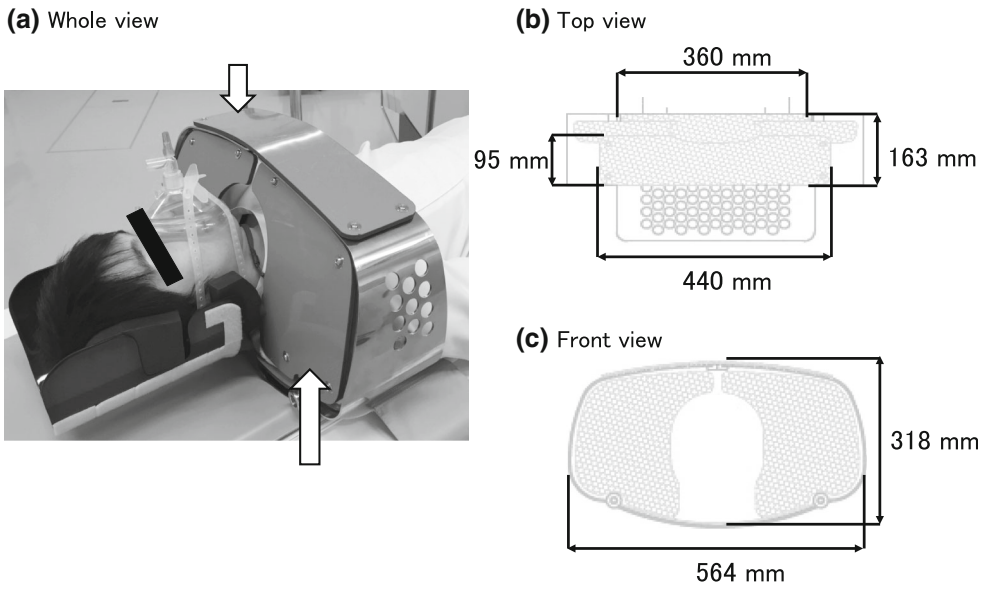

Fig. 1 Novel tungsten-impregnated rubber neck shield with stainless alloy frame. Whole (**a**), top (**b**), and front (**c**) views. *Arrows* tungsten-impregnated rubber

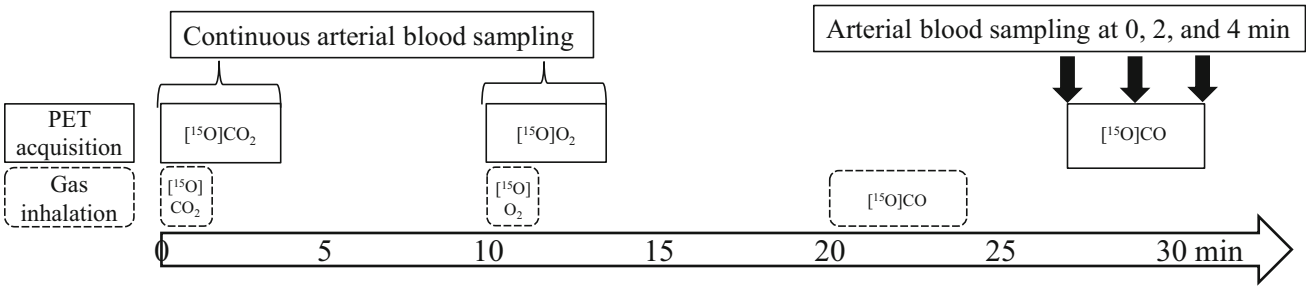

Fig. 2 Schema of ^{15}O-labeled gas study using a positron emission tomography (PET) auto-radiographic method

[^{15}O]CO images were acquired for 4 min after 3 min of [^{15}O]CO gas inhalation. The interval between each gas inhalation was 10 min.

The amount of radioactivity in arterial whole blood was continuously measured via arterial puncture by a physician using a BeCON Model 01 Gd_2SiO_5:Ce (GSO) coincidence detector (Molecular Imaging Labo, Suita, Japan) while the images of inhaled [^{15}O]CO_2 and [^{15}O]O_2 were acquired [25]. The amount of radioactivity was measured in samples of arterial whole blood (1.0 mL) that were manually collected at 0, 2, and 4 min during the acquisition of PET images of [^{15}O]CO inhalation using a BeWell Model-QS03 F/B well counter (Molecular Imaging Labo, Suita, Japan).

2.5 Data processing

PET images were reconstructed under the following conditions: three-dimensional-ordered-subsets expectation–maximization (3D-OSEM) algorithm, 128 × 128 matrix, 47 slices, 2.0 mm/pixel, 3.27 mm/slice, 4 iterations, 16 subsets, and Gaussian filter of 3.0 mm (FWHM). The clinical [^{15}O]CO_2 and [^{15}O]O_2 images consisted of 12 frames of 5 s and 10 frames of 15 s. Attenuation was corrected using the corresponding CT image. We applied scatter limitation correction (SLC) to correct the SC error derived from high levels of radioactive ^{15}O gas inside a facemask [23, 26]. The SLC limits the amount of scatter outside the object when the scatter fraction of the emission profile exceeds a specific threshold and allows SC scaling to levels typical of clinical PET images. That is, significantly scaled scatter profiles are scaled down by adjusting the amount of scatter outside the object in the process of single scatter simulation [26]. We calculated the CBF, CBV, OEF, and $CMRO_2$ from functional images and amounts of radioactivity in arterial blood using the PET autoradiographic method with Xeleris software (GE Healthcare, Milwaukee, WI, USA) [3].

2.6 Data analysis

2.6.1 PET count rate characteristics

Noise equivalent count rates (NECRs) [27] were calculated as follows:

$$\mathrm{NECR} = (1 - \mathrm{SF})^2 \frac{(T+S)^2}{(T+S)+R}\,[\mathrm{cps}],$$

where SF is the scatter fraction, T is the true coincidence count rate, S is the scatter coincidence count rate, and R is the random coincidence count rate. We calculated $(T + S)$ by subtracting the random from the prompt coincidence count rate (P). The NECR was calculated for the image sequences of each gas in the clinical study. We calculated NECR gain as NECR with/without the neck shield. Values for P, R, $(T + S)$, and NECR in each frame of $[^{15}O]CO_2$ and $[^{15}O]O_2$ images with and without the neck shield in the clinical study were compared using the Wilcoxon matched-pairs signed rank test. Values of $p < 0.05$ were considered significant.

2.6.2 Image uniformity

Circular regions of interest (ROIs) of 18 cm in diameter were placed on all slices of the center of the head-simulated phantom images to determine mean radioactivity (kBq/mL) and standard deviation (SD). The coefficient of variance (CV) to evaluate image uniformity for each slice was calculated as

$$\mathrm{CV}_i = {}^{\mathrm{SD}_i}/_{\text{mean radioactivity}_i} \times 100(\%),$$

where i is the slice number. The radioactivity concentration and CVs between with and without the neck shield were compared using the Wilcoxon matched-pairs signed rank test. Values of $p < 0.05$ were considered significant.

2.6.3 Variation of voxel value

Circular ROIs with a 10-mm diameter were placed manually on three adjacent slices of CBF, CBV, OEF, and $CMRO_2$ images (24 ROIs per region) of the cerebellar cortex and frontal, temporal, and occipital lobes in the clinical study (Fig. 3). The SDs inside ROIs from images of the three participants were measured. The average SD of functional images was calculated from all SDs from the three participants. We calculated SD change from the ratio of average SD with and without the neck shield. We compared SDs with and without the neck shield using paired t tests. Values of $p < 0.05$ were considered significant. All ROIs were analyzed using Dr. View/Linux (AJS, Tokyo, Japan).

2.6.4 Inter-acquisition variability

We also compared the mean value, SD, and CV (SD/mean value) of quantitative metrics of CBF (mL/100 g/min), CBV (mL/100 g), OEF (%), and $CMRO_2$ (mL/100 g/min) in each region with and without the neck shield.

3 Results

3.1 PET count rate characteristics

Table 1 shows the PET count characteristics in the phantom and clinical studies. The neck shield decreased the prompt and random count rates by 37.1 and 58.8%, respectively, and increased the true + scatter count rate and NECR by 15.0 and 61.3%, respectively, in the phantom study. Prompt and random count rates in the clinical study were decreased by 9.5 and 24.5% in $[^{15}O]CO_2$ images, by 22.1 and 36.3% in $[^{15}O]O_2$ images, and by 20.8 and 44.9% in $[^{15}O]CO$ images, respectively. The neck shield significantly decreased the prompt and random count rates of $[^{15}O]CO_2$ and $[^{15}O]O_2$. The true + scatter count rates and NECRs were increased by 14.2 and 43.9%, 15.5 and 65.9%, and 9.3 and 55.0% in the $[^{15}O]CO_2$, $[^{15}O]O_2$, and $[^{15}O]CO$ images, respectively. True + scatter count rates and NECRs were significantly increased with the neck shield except for the true + scatter count rate in the $[^{15}O]CO_2$ images. The count characteristics of the clinical $[^{15}O]CO$ images tended to be the same as those of the other images, i.e. the difference was not statistically significant. The values of the scatter fraction were not different between with the neck shield and without the neck shield in the phantom and clinical studies.

3.2 Image uniformity

Figure 4 shows the mean radioactivity of all ROIs in the phantom study with and without the neck shield. The mean radioactivity was lower in caudal slices than in cranial slices. The average of mean radioactivity and the CV of all ROIs with and without the neck shield were 12.2 ± 0.1 kBq/mL and $15.4 \pm 8.2\%$, and 11.1 ± 0.1 kBq/mL and $16.3 \pm 8.8\%$, respectively. The neck shield significantly decreased radioactivity concentration and CV (both $p < 0.05$). The ratio of injected radioactivity in the phantom with and without the neck shield was equivalent to the ratio of mean radioactivity concentration in the phantom image with to that without the neck shield.

3.3 Variation of voxel value

Table 2 shows the average SDs with and without the neck shield and SD change using the neck shield in functional images. The neck shield significantly decreased SD in the $CMRO_2$ images ($p < 0.05$). Further, the SD of the cerebellum region in the CBF images, occipital region in the CBV images, and all regions in the $CMRO_2$ images decreased significantly with the neck shield ($p < 0.05$). There was no change in SD after using the neck shield in

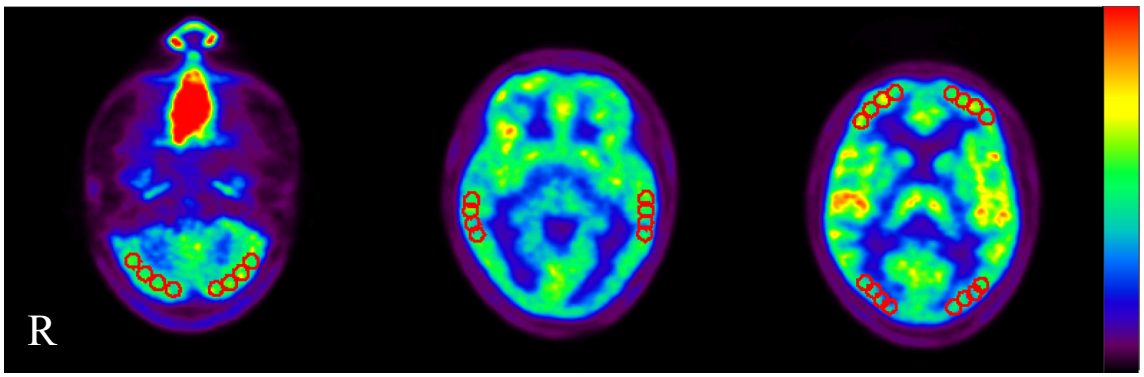

Fig. 3 Location of regions of interest (ROI) on cerebral blood flow images. *Circular* 10-mm ROI are set on three adjacent slices

Table 1 PET count characteristics in phantom and clinical studies

	Prompt (Mcps)	Random (Mcps)	True + scatter (Mcps)	Scatter fraction	NECR (kcps)	NECR gain
Phantom						
Without shield	1.07	0.75	0.32	0.29	69.3	1.61
With shield	0.67	0.31	0.36	0.28	111.8	
Clinical						
[^{15}O]CO_2 ($n = 3$)						
Without shield	1.61 ± 0.43	0.98 ± 0.28	0.62 ± 0.15	0.28 ± 0.02	123.7 ± 31.8	1.44
With shield	1.45 ± 0.46*	0.74 ± 0.29*	0.71 ± 0.18	0.29 ± 0.02	178.0 ± 43.0	
[^{15}O]O_2 ($n = 3$)						
Without shield	1.38 ± 0.39	1.00 ± 0.28	0.38 ± 0.12	0.29 ± 0.02	54.3 ± 21.4	1.66
With shield	1.07 ± 0.31*	0.64 ± 0.20*	0.43 ± 0.10*	0.29 ± 0.02	90.1 ± 23.6*	
[^{15}O]CO ($n = 3$)						
Without shield	0.20 ± 0.05	0.11 ± 0.04	0.09 ± 0.03	0.31 ± 0.01	18.9 ± 5.8	1.55
With shield	0.16 ± 0.07	0.06 ± 0.04	0.10 ± 0.04	0.31 ± 0.01	29.3 ± 9.1	

NECR noise equivalent count rate

* Significant difference from values obtained without neck shield (Wilcoxon matched pairs signed rank test, $p < 0.05$)

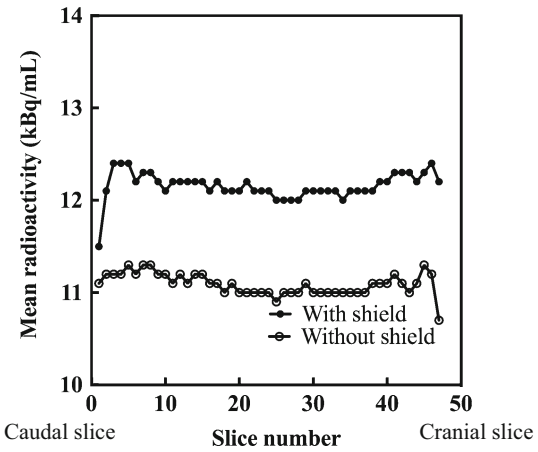

Fig. 4 Mean radioactivity of slices in a head phantom with and without the neck shield. *Black and white circles* with and without the neck shield, respectively

the entire CBF, CBV, and OEF images, nor were there region-specific changes. Figure 5 shows the CBF, CBV, OEF, and $CMRO_2$ images from a participant with and without the neck shield. The image noise on functional images with the neck shield was the same as that without it.

3.4 Inter-acquisition variability

The mean ± SD of the quantitative parameters of CBF, CBV, OEF, and $CMRO_2$ in total region with and without the neck shield were 54.5 ± 11.8 and 55.7 ± 14.8 mL/100 g/min; 3.3 ± 1.1 and 3.4 ± 1.1 mL/100 g; 36.2 ± 3.4 and 38.3 ± 5.0%; and 6.3 ± 2.3 and 8.1 ± 3.5 mL/100 g/min, respectively. Table 3 shows the SD and CV of quantitative parameters of CBF, CBV, OEF, and $CMRO_2$ in each region with and without the neck shield.

Table 2 SDs (mean ± SD) and SD changes of CBF, CBV, OEF, and $CMRO_2$ with and without neck shield

Region	CBF ($n = 3$)		CBV ($n = 3$)		OEF ($n = 3$)		$CMRO_2$ ($n = 3$)	
	Without shield	With shield	Without shield	With shield	Without shield	With shield	Without shield	With shield
Cerebellum	9.0 ± 3.0*	7.4 ± 2.6*	0.9 ± 0.5	1.0 ± 0.6	4.1 ± 1.2	4.3 ± 1.4	1.0 ± 0.4*	0.7 ± 0.3*
Frontal	8.2 ± 3.1*	8.7 ± 3.3*	0.6 ± 0.2*	0.8 ± 0.3*	3.0 ± 0.9	2.9 ± 1.0	1.2 ± 0.6*	1.1 ± 0.6*
Temporal	7.4 ± 2.9	7.0 ± 2.8	1.2 ± 0.7	1.3 ± 0.6	3.4 ± 1.1	3.1 ± 0.9	1.0 ± 0.4*	0.7 ± 0.3*
Occipital	13.1 ± 7.6*	14.1 ± 8.0*	1.2 ± 0.7*	0.9 ± 0.3*	10.9 ± 7.9	10.2 ± 7.1	2.9 ± 2.2*	2.2 ± 1.6*
Total	9.7 ± 4.9	9.8 ± 5.3	1.0 ± 0.6	1.0 ± 0.5	6.3 ± 4.7	6.0 ± 4.4	1.8 ± 1.3*	1.4 ± 1.0*
SD change of total region	0.99		1.01		1.05		1.28	

SD standard deviation, *CBF* cerebral blood flow, *CBV* cerebral blood volume, *OEF* oxygen extraction fraction, $CMRO_2$ cerebral metabolic rate of oxygen

* Significant difference from values obtained without neck shield (paired t test, $p < 0.05$)

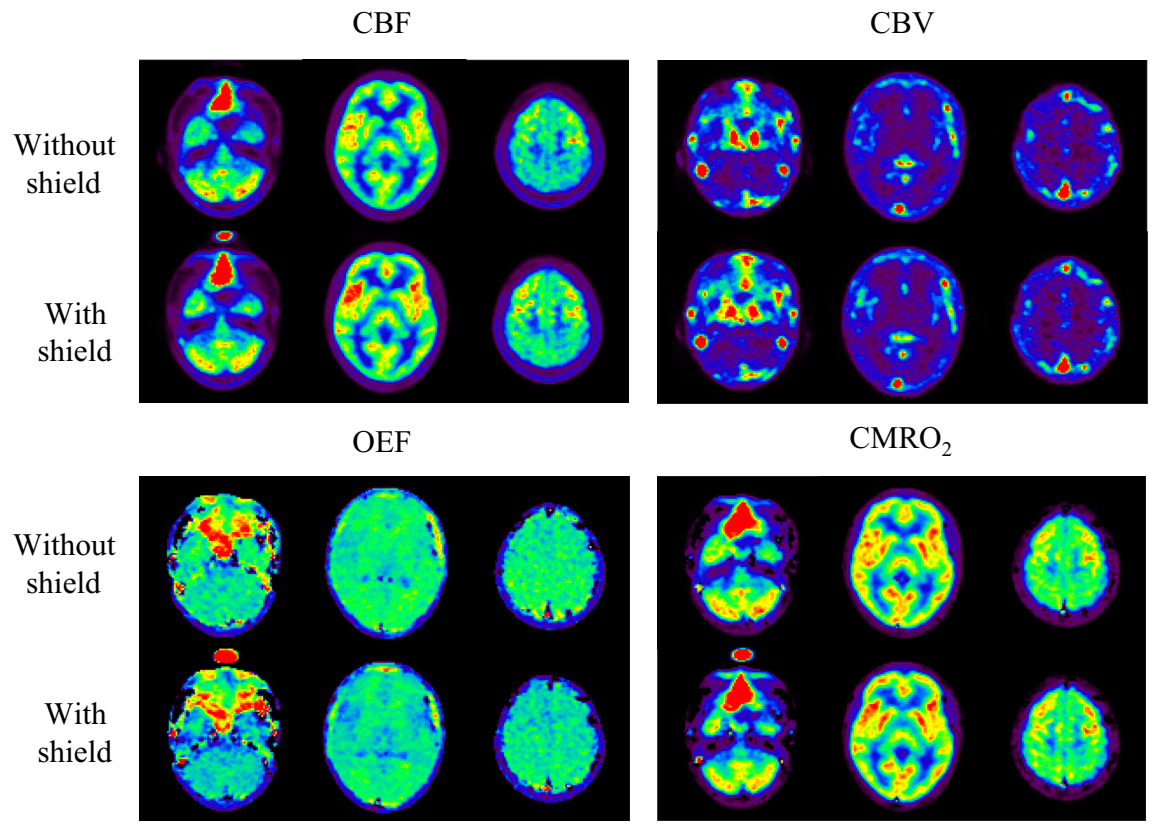

Fig. 5 Parametric images of cerebral blood flow (*CBF*), cerebral blood volume (*CBV*), oxygen extraction fraction (*OEF*), and cerebral metabolic rate of oxygen ($CMRO_2$) with and without the neck shield. *Color scales* in the CBF and $CMRO_2$ images represent 0–80% of the maximum value. The ranges of the color scales in the CBV and OEF images are 0–20 (mL/100 g) and 0–80 (%), respectively

4 Discussion

We investigated the ability of a novel neck shield made of tungsten-impregnated rubber to improve the quality of ^{15}O-labeled gas images acquired using 3D PET/CT. The neck shield improved NECRs from 43.9 to 65.9% by reducing random coincidence in the phantom and clinical studies. However, an improvement of physical and visual image quality with the neck shield was not observed in the phantom and clinical studies.

Radioactivity outside the FOV degrades 3D PET whole-body and brain image quality and quantitation [10–16]. A neck shield reduces direct and scattered photons from outside of the FOV and improves count rate performance

Table 3 Inter-acquisition variability with and without the neck shield in each region

Quantitative parameter	Region	Mean	SD	CV (%)
CBF ($n = 3$) [mL/100 g/min]	Cerebellum	62.3	7.6	12.3
	Frontal	55.9	5.4	9.5
	Temporal	58.4	6.3	10.8
	Occipital	44.2	4.4	10.1
CBV ($n = 3$) [mL/100 g]	Cerebellum	3.3	0.7	20.3
	Frontal	3.0	0.4	12.0
	Temporal	4.4	1.1	26.2
	Occipital	2.8	0.5	18.5
OEF ($n = 3$) [%]	Cerebellum	35.9	2.6	7.3
	Frontal	37.9	2.8	7.3
	Temporal	37.8	3.5	9.4
	Occipital	37.2	3.3	9.0
$CMRO_2$ ($n = 3$) [mL/100 g/min]	Cerebellum	7.8	1.5	19.4
	Frontal	7.6	1.3	16.8
	Temporal	7.7	1.4	18.2
	Occipital	5.9	0.9	15.5

CBF cerebral blood flow, *CBV* cerebral blood volume, *OEF* oxygen extraction fraction, *$CMRO_2$* cerebral metabolic rate of oxygen, *SD* standard deviation, *CV* coefficient of variation

[11, 15, 17–19]. Thompson and Moreno-Cantu found that an additional shield during brain PET imaging with [^{11}C]raclopride, [^{15}O]H_2O, and [^{18}F]FDG improved NEC in three studies. They concluded that the additional shield conferred the greatest benefit upon [^{15}O]H_2O or ^{15}O-oxygen images [19]. Spinks et al. also found that an additional shield improved PET count rates, more so in head than in body images [11]. Our phantom and clinical results showed that the random count rate of [^{15}O]O_2 decreased to 36.3% and that the NECR increased to 65.9% using the neck shield. Ibaraki et al. [15] showed that random counts were reduced by about 40% and NECR increased by about 40% when a 7-mm lead-plate neck shield was applied during [^{15}O]O_2 image acquisition [19]. Our PET count characteristics using a tungsten-impregnated rubber neck shield with a lead equivalent of 6 mm were similar to those reported by Ibaraki et al. [15]. The values of scatter fraction were not much different with and without the neck shield. The radioactivity outside the FOV was found to have no effect on the scatter fraction in a previous study [14]. Our findings suggest that the benefit of the neck shield is in the reduction of random counts. Our PET/CT scanner exhibited higher count rates and decreased dead time because the scanner uses LYSO, in which fluorescence decays faster than the GSO used by Ibaraki et al. [15]. The NECR results suggested that the quality of PET images acquired using an LYSO scanner and ^{15}O-labeled gas is not degraded by scatter photons from outside the FOV.

The variation of voxel value of $CMRO_2$ decreased significantly upon using the neck shield, although the $CMRO_2$ image did not improve visually. The neck shield not only improved the statistical noise in functional images in the clinical study but also the parameters of image quality such as CV in the phantom study. Ibaraki et al. showed that a neck shield improved SNR calculated using the bootstrap method by about 20% [15]. The neck shield did not improve measures of image quality such as CV and SD in the present study because our iterative 3D-OSEM method of reconstruction might produce less image noise without the neck shield, compared to other methods.

Thus, the quality of functional images was equivalent between the procedures done with and without the neck shield when the PET system included an LYSO scanner and the reconstruction method was 3D-OSEM. The relationship between the count characteristics and image quality is nonlinear when using 3D-OSEM in a PET/CT scanner that does not correct for scatter and random events by subtraction of the estimated scatter and random events, respectively [28]. Furthermore, the improvements of image quality based on SD change were slight in comparison with NECR gain in our study.

In the phantom study, the difference of mean radioactive concentration with and without the neck shield was equivalent to the difference in injected dose in the phantom with and without the neck shield. Thus, we demonstrated that the neck shield did not affect the quality and quantity of ^{15}O-labeled gas images from the phantom study. However, the range of CVs, which represent the inter-acquisition variability between acquisitions with and without the neck shield, was 9.5–12.3%, 12.0–26.2%, 7.3–9.4%, and 15.5–19.4% in the CBF, CBV, OEF, and $CMRO_2$, respectively. The inter-acquisition variability of CBV and

$CMRO_2$ was worse than those found in a previous study [29]. Although we defined the ROIs to exclude large blood vessels in the CBV image, spillover from small blood vessels contained in ROIs might have degraded the inter-acquisition variability. Further, the quantitative parameter of $CMRO_2$ was calculated from the CBV images, meaning that the inter-acquisition variability of $CMRO_2$ might also be degraded.

The present study has two limitations. One is that the sample size of three participants was insufficient to establish definite evidence. The other is that some technologies such as point-spread-function [30], time-of-flight [31], and a novel reconstruction algorithm [32] might also improve the image quality of ^{15}O-labeled gas imaging. We did not make comparisons with these various other correction methods.

5 Conclusion

A tungsten-impregnated rubber neck shield reduced the random count rate and improved count-based SNR such as NECR in a 3D PET study using ^{15}O-labeled gas. The image quality with the neck shield was as same as that without the neck shield. The neck shield is useful in terms of improvement of count rate performance, and our PET system and acquisition condition without the neck shield is applicable to qualitative and quantitative ^{15}O-labeled gas PET imaging.

Acknowledgements We would like to thank Mr. Kunpei Hayashi and Mr. Rokuya Hayashi for technical support with the cyclotron operation and radiosynthesis, and Ms. Hatsumi Endo for care of subjects during the PET scanning.

Compliance with ethical standards

Ethical statement Data were obtained without including any personal information concerning the subjects in this study, so there was no conflict with the Ethical Guidelines for Clinical Research.

Conflict of interest The authors have no conflicts of interest to declare.

Informed consent Informed consent was obtained from all participants included in the study.

Funding source information This research received no specific grant from any funding agency in the public, commercial, or not-for-profit sectors.

References

1. Mintun MA, Raichle ME, Martin WR, Herscovitch P. Brain oxygen utilization measured with O-15 radiotracers and positron emission tomography. J Nucl Med. 1984;25(2):177–87.
2. Sadato N, Yonekawa Y, Senda M, Iwasaki Y, Matoba N, Tamaki N, et al. PET and the autoradiographic method with continuous inhalation of oxygen-15-gas: theoretical analysis and comparison with conventional steady-state methods. J Nucl Med. 1993;34(10):1672–80.
3. Shidahara M, Watabe H, Kim KM, Oka H, Sago M, Hayashi T, et al. Evaluation of a commercial PET tomograph-based system for the quantitative assessment of rCBF, rOEF and $rCMRO_2$ by using sequential administration of ^{15}O-labeled compounds. Ann Nucl Med. 2002;16(5):317–27.
4. Yamauchi H, Fukuyama H, Nagahama Y, Nabatame H, Nakamura K, Yamamoto Y, et al. Evidence of misery perfusion and risk for recurrent stroke in major cerebral arterial occlusive diseases from PET. J Neurol Neurosurg Psychiatry. 1996;61(1):18–25.
5. Yamauchi H, Fukuyama H, Nagahama Y, Nabatame H, Ueno M, Nishizawa S, et al. Significance of increased oxygen extraction fraction in five-year prognosis of major cerebral arterial occlusive diseases. J Nucl Med. 1999;40(12):1992–8.
6. Kobayashi M, Okazawa H, Tsuchida T, Kawai K, Fujibayashi Y, Yonekura Y. Diagnosis of misery perfusion using noninvasive ^{15}O-gas PET. J Nucl Med. 2006;47(10):1581–6.
7. Matsumoto Y, Ogasawara K, Saito H, Terasaki K, Takahashi K, Ogasawara Y, et al. Detection of misery perfusion in the cerebral hemisphere with chronic unilateral major cerebral artery steno-occlusive disease using crossed cerebellar hypoperfusion: comparison of brain SPECT and PET imaging. Eur J Nucl Med Mol Imaging. 2013;40(10):1573–81.
8. Lartizien C, Comtat C, Kinahan PE, Ferreira N, Bendriem B, Trébossen R. Optimization of injected dose based on noise equivalent count rates for 2- and 3-dimensional whole-body PET. J Nucl Med. 2002;43(9):1268–78.
9. Visvikis D, Griffiths D, Costa DC, Bomanji J, Ell PJ. Clinical evaluation of 2D versus 3D whole-body PET image quality using a dedicated BGO PET scanner. Eur J Nucl Med Mol Imaging. 2005;32(9):1050–6.
10. Sossi V, Barney JS, Harrison R, Ruth TJ. Effect of scatter from radioactivity outside of the field of view in 3D PET. IEEE Trans Nucl Sci. 1995;42:1157–61.
11. Spinks TJ, Miller MP, Bailey DL, Bloomfield PM, Livieratos L, Jones T. The effect of activity outside the direct field of view in a 3D-only whole-body positron tomograph. Phys Med Biol. 1998;43(4):895–904.
12. Hasegawa T, Suzuki M, Murayama H, Irie T, Fukushi K, Wada Y. Influence of radioactivity out of the field of view on 3D PET dynamic measurement with [^{11}C]MP4A. IEEE Trans Nucl Sci. 1999;46:1087–92.
13. Ibaraki M, Miura S, Shimosegawa E, Sugawara S, Mizuta T, Ishikawa A, et al. Quantification of cerebral blood flow and oxygen metabolism with 3-dimensional PET and ^{15}O: validation by comparison with 2-dimensional PET. J Nucl Med. 2008;49(1):50–9.
14. Matheoud R, Secco C, Della Monica P, Leva L, Sacchetti G, Inglese E, et al. The effect of activity outside the field of view on image quality for a 3D LSO-based whole body PET/CT scanner. Phys Med Biol. 2009;54(19):5861–72.
15. Ibaraki M, Sugawara S, Nakamura K, Kinoshita F, Kinoshita T. The effect of activity outside the field-of-view on image signal-to-noise ratio for 3D PET with (^{15})O. Phys Med Biol. 2011;56(10):3061–72.
16. Kloet RW, de Jong HWAM, van Velden FHP, Lammmertsma AA, Boellard R. Influence of outside field of view activity on the quality of high resolution research tomograph (HRRT) brain studies. IEEE Nucl Sci Symp Conf Record. 2006;6:3369–71.
17. Thompson CJ, Kecani S, Boelen S. Evaluation of a neck shield for use during neurological studies with a whole-body PET scanner: IEEE Trans Nucl Sci. 2001;48:1512–7.

18. Hasegawa T, Murayama H, Matsuura H, Yamaya T. A Phantom and simulation study on body-shields to cope with radioactivity outside the field of view in 3D PET. IEEE Trans Nucl Sci. 2001;48:1267–71.
19. Thompson CJ, Moreno-Cantu JJ. Measurement of the change in noise-effective count rate during PET brain studies with additional shielding. IEEE Trans Nucl Sci. 2002;49(5):2057–61.
20. Pepin CM, Berard P, Perrot AL, Pepin C, Houde D, Lecomte R, et al. Properties of LYSO and recent LSO scintillators for phoswich PET detectors. IEEE Trans Nucl Sci. 2004;51(3):789–95.
21. Bettinardi V, Presotto L, Rapisarda E, Picchio M, Gianolli L, Gilardi MC. Physical performance of the new hybrid PET/CT Discovery-690. Med Phys. 2011;38(10):5394–411.
22. National Electrical Manufactures Association. Performance measurements of positron emission tomographs. NEMA Standards Publication NU-2 2007. Rosslyn: NEMA; 2007
23. Hori Y, Hirano Y, Koshino K, Moriguchi T, Iguchi S, Yamamoto A, et al. Validity of using a 3-dimensional PET scanner during inhalation of ^{15}O-labeled oxygen for quantitative assessment of regional metabolic rate of oxygen in man. Phys Med Biol. 2014;59(18):5593–609.
24. Shidahara M, Watabe H, Kim KM, Kudomi N, Ito H, Iida H. Optimal scan time of oxygen-15-labeled gas inhalation autoradiographic method for measurement of cerebral oxygen extraction fraction and cerebral oxygen metabolic rate. Ann Nucl Med. 2008;22(8):667–75.
25. Kudomi N, Choi E, Watabe H, Kim KM, Shidahara M, Ogawa M, et al. Development of a GSO detector assembly for a continuous blood sampling system. IEEE Trans Nucl Sci. 2003;50:70–3.
26. Miwa K, Umeda T, Murata T, Wagatsuma K, Miyaji N, Terauchi T, et al. Evaluation of scatter limitation correction: a new method of correcting photopenic artifacts caused by patient motion during whole-body PET/CT imaging. Nucl Med Commun. 2016;37(2):147–54.
27. Fukukita H, Suzuki K, Matsumoto K, Terauchi T, Daisaki H, Ikari Y, et al. Japanese guideline for the oncology FDG-PET/CT data acquisition protocol: synopsis of Version 2.0. Ann Nucl Med. 2014;28(7):693–705.
28. Chang T, Chang G, Clark JW, Diab RH, Rohren E, Mawlawi OR. Reliability of predicting image signal-to-noise ratio using noise equivalent count rate in PET imaging. Med Phys. 2012;39(10):5891–900.
29. Bremmer JP, van Berckel BN, Persoon S, Kappelle LJ, Lammertsma AA, Kloet R, et al. Day-to-day test-retest variability of CBF, CMRO2, and OEF measurements using dynamic ^{15}O PET studies. Mol Imaging Biol. 2011;13(4):759–68.
30. Varrone A, Sjöholm N, Eriksson L, Gulyás B, Halldin C, Farde L. Advancement in PET quantification using 3D-OP-OSEM point spread function reconstruction with the HRRT. Eur J Nucl Med Mol Imaging. 2009;36:1639–50.
31. Nagaki A, Onoguchi M, Matsutomo N. Clinical validation of high-resolution image reconstruction algorithms in brain ^{18}F-FDG-PET: effect of incorporating Gaussian filter, point spread function, and time-of-flight. Nucl Med Commun. 2014;35(12):1224–32.
32. Teoh EJ, McGowan DR, Macpherson RE, Bradley KM, Gleeson FV. Phantom and clinical evaluation of the Bayesian penalized likelihood reconstruction algorithm Q.Clear on an LYSO PET/CT system. J Nucl Med. 2015;56(9):1447–52.